Proceedings of SPIE's 7th Annual International Symposium on Smart Structures and Materials, 1-5 March, 2000, Newport, CA. Paper No. 3992-103

Complete Modeling of Rotary Ultrasonic Motors Actuated By Traveling Flexural Waves

Xiaoqi Bao and Yoseph Bar-Cohen
Jet Propulsion Laboratory, Caltech, Pasadena, CA 91109, yosi@jpl.nasa.gov

ABSTRACT

Ultrasonic rotary motors have the potential to meet this NASA need and they are developed as actuators for miniature telerobotic applications. These motors are being adapted for operation at the harsh space environments that include cryogenic temperatures and vacuum and analytical tools for the design of efficient motors are being developed. A hybrid analytical model was developed to address a complete ultrasonic motor as a system. Included in this model is the influence of the rotor dynamics, which was determined experimentally to be important to the motor performance. The analysis employs a 3D finite element model to express the dynamic characteristics of the stator with piezoelectric elements and the rotor. The details of the stator including the teeth, piezoelectric ceramic, geometry, bonding layer, etc. are included to support practical USM designs. A brush model is used for the interface layer and Coulomb's law for the friction between the stator and the rotor. The theoretical predictions were corroborated experimentally for the motor. In parallel, efforts have been made to determine the thermal and vacuum performance of these motors. To explore telerobotic applications for USMs a robotic arm was constructed with such motors.

Keywords: Piezoelectric Motors, Ultrasonic Motors (USMs), Stators and Rotors, Modal Analysis, Actuators, Active Materials

1. INTRODUCTION

Actuators are used to operate NASA telerobotic devices that include robotic arms and rovers, as well as space mechanism and instruments such as release mechanisms, antenna and instrument deployment, positioners, aperture opening and closing devices. Increasingly, efforts are made to seek actuators that are compact, lightweight and miser. These constraints are necessary to allow meeting growing mission requirements with as many experiments and tasks as possible while conforming to strict mass, size, power, and cost allocations. This trend is straining the specifications of actuation and articulation mechanisms that drive space and planetary instruments. The miniaturization of conventional electromagnetic motors is limited by practical manufacturing difficulties. These types of motors are compromising speed for torque using speed-reducing gears. The use of gear adds mass, volume and complexity as well as decreases the motor drive system reliability due the involvement of a larger number of system components. The recent introduction of rotary ultrasonic motors (USMs) enabled a new effective actuator for drive mechanisms of miniature instruments [Hollerbach, et al 1991, Flynn, 1992, E. Inaba, et al, 1995, Wallashek, 1995, and Uchino 1998]. These motors have high torque density at low speed, high holding torque, simple construction, and have a quick response. JPL is developing these motors for operation at such planetary environments as Mars over an extended period, where the temperature is as low as -120° C and cyclically changing over range of many tens of degrees between day and night while the ambient pressure is about 6-torr. This range of temperatures and pressures is beyond the specifications of commercial piezoelectric motors even though there is no technical reason why these motors would not work. An alternative stator drive approach was developed to enhance the longevity and planetary operability of these motors. A theoretical model was developed to allow predicting the response of the stator to various drive frequencies and the results were corroborated experimentally.

Generally, ultrasonic motors [Wallashek, 1995] can be classified by their mode of operation (static or resonant), type of motion (rotary or linear) and shape of implementation (beam, rod, disk, etc.). Despite the distinctions, the fundamental principles of solid-state actuation tie them together: microscopic material deformations (usually associated with piezoelectric materials) are amplified through either quasi-static mechanical or dynamic/resonant means. Several of the motor classes have seen commercial application in areas needing compact, efficient, and intermittent motion. Such

applications include: camera auto-focus lenses, watch motors and compact paper handling. Obtaining the levels of torque-speed characteristics of USMs using conventional motors requires adding a gear system to reduce the speed, thus increasing the size, mass and complexity of the drive mechanism. USMs are fundamentally designed to have a high holding force, providing effectively zero backlash. Further, since these motors are driven by friction the torque that would cause them to be backdriven at zero power is significantly higher than the stall torque. The number of components needed to construct ultrasonic motor is small minimizing the number of potential failure points. The general characteristic of USMs makes them attractive for robotic applications where small, intermittent motions are required.

In Figure 1 the principle of operation of an ultrasonic motor (flexural traveling wave ring-type motor) is shown as an example. A traveling wave is established over the stator surface, which behaves as an elastic ring, and produces elliptical motion at the interface with the rotor. This elliptical motion of the contact surface propels the rotor and the drive-shaft connected to it. Teeth on the top section of the stator are intended to form a moment arm to amplify the speed. The operation of USM depends on friction at the interface between the moving rotor and stator, which is a key issue in the design of this interface for extended lifetime.

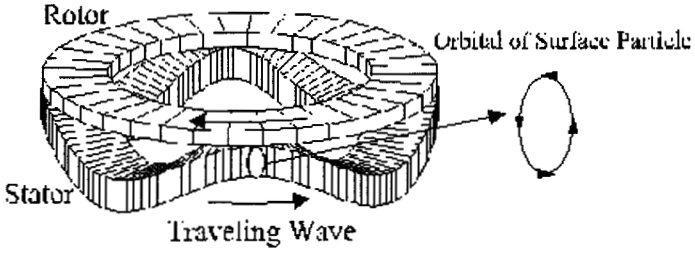

Figure 1: Principle of operation of a rotary flexural traveling wave motor.

2. HYBIRD MODELING OF USM BASED ON FINITE ELEMENT APPROACH

In a previous paper [Bar-Cohen, 1999], finite element model for the stator was reported. Although the stator is the key part of the motor. However, both mathematical and experimental studies show that the characteristics of the rotor and the friction layer also have important influence to the performance of the motor [Maeno, 1994 and Hagedorn, et al, 1998]. To predict the motor performance with reasonable accuracy for motor design, a hybrid analytical model was developed to address a complete ultrasonic motor as a system. The analysis employs a 3D finite element model to express the dynamic characteristics of the stator with piezoelectric elements and the rotor. The details of the stator including the teeth, piezoelectric ceramic, geometry, bonding layer, etc. are included to support practical USM designs. The rotor is modeled by annular finite element. A brush model is used for the interface layer and Coulomb's law for the friction between the stator and the rotor. The stator and the rotor are interacted via the interface layer.

2.1 The Stator

The structure of the stator that we modeled is presented in Figure 2, which includes PZT ring, bonding layer and a metal disk with varied cross section and teeth. The electrodes of the PZT ring are patterned to excite 5-wave mode vibration of the stator. To generate traveling wave, the poling direction of the piezoelectric ceramic is structured such that a quarter wavelength out-of-phase is formed. This poling pattern is also intended to eliminate extension in the stator and maximize bending. The teeth on the stator are arranged in a ring at the radial position. To generate a traveling wave within the stator two orthogonal modes are activated simultaneously. These modes are induced by a stator that is constructed with the drive piezoelectric elements in the form of two sections of poling pattern that are bonded to the stator. Geometrical examination of this pattern shows that driving the two sections using $cos(\omega t)$ and $sin(\omega t)$ signals, respectively, will produce a traveling wave with a frequency of $\omega/2\pi$. Also, by changing the sign on one of the drive signals, the traveling wave would reveres its direction.

The equation of motion of an elastic structure including piezoelectric elements can be derived from Hamilton's principle. The finite element model for piezoelectric vibration has been derived by many authors (e.g. Allik et al, Kagawa et al). The discretized equation of the stator can be expressed as

$$[M]\{\ddot{\xi}\} + [C]\{\dot{\xi}\} + [K]\{\xi\} = [P]\{\varphi\} + \{F\}$$

$$[P]^T\{\xi\} - [G]\{\varphi\} = \{Q\} \tag{1}$$

where [M], [C], [K], [P], [G], are the mass, damping, stiffness, electromechanical coupling, and capacitance matrices, respectively. The vectors {ξ}, {φ}, {F}, and {Q} are the nodal displacement, the electric potential vectors the normal external force, the tangential external force and the charge vectors, respectively. For simple harmonic motion, we have

$$\begin{aligned} &([K] + j\omega[C] - \omega^2[M])\{\xi\} - [P]\{\varphi\} = \{F\} \\ &[P]^T\{\xi\} - [G]\{\varphi\} = \{Q\} \end{aligned} \tag{2}$$

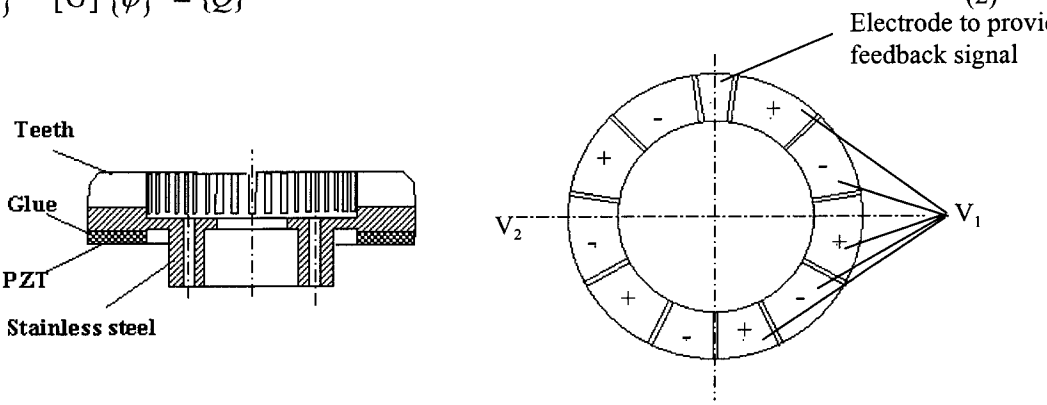

(a) Stator of piezoelectric motor **(b) PZT ring**

Figure 2: Piezoelectric stator and PZT ring

The charge at all nodes (not on the electrodes) is zero and the electric potentials at the nodes on the same electrode are equal to each other. Therefore, we have constraints as

$$\begin{aligned} q_1 = q_2 = \ldots = 0 \quad &\text{for nodes not on electrodes} \\ \varphi_1 = \varphi_2 = \ldots = V_e \quad &\text{for nodes on electrodes} \end{aligned} \tag{3}$$

where V_e is the voltage on electrode *e*.

The modal analysis is used to analyze the resonance of the stator, determine the resonance frequencies and mode shapes by assigning zero to [C], {F} and all V_e and solving the eigenvalue problem of Eq. (2) with constraint (3). We have normalized mode shapes

$$\{\xi_1\}, \{\xi_2\}, \ldots, \{\xi_n\}$$

$$\text{with} \quad \{\xi_i\}^*[M]\{\xi_i\} = 1 \tag{4}$$

and corresponding resonance frequencies,

$$\omega_1, \omega_2, \ldots, \omega_n \tag{5}$$

When the motor operated near particular mode frequencies, these modes are dominated. We only take these modes in count in the analysis. For the stator, only two modes, say $\{\xi_1\}$ and $\{\xi_2\}$, which are exited to form the traveling wave are considered. These two modes have the same frequency $\omega_1 = \omega_2 = \omega_0$ and same mode shape except separated by $\lambda/4$ in space. The equations for the modes are written as [Bao 1988]

$$(\omega_0^2 + j\omega R - \omega^2)d_i = pV_i + Fm_i$$
$$Q_i = pd_i + C_0V_i \tag{6}$$

where d_i is the amplitude of the mode i, R, p and Fm are generalized damping, electromechanical coupling and force respectively.

It is more convenient to take traveling wave modes as basic functions. The traveling wave modes are presented as

$$\{\eta_1\} = \{\xi_1\} - j\{\xi_2\}$$
$$\{\eta_2\} = \{\xi_1\} + j\{\xi_2\} \tag{7}$$

and the components u of the traveling modes satisfy the following equations

$$(\omega_0^2 + j\omega R - \omega^2)u_1 = \frac{1}{2}p(V_1 + jV_2) + Fs_1 \tag{8}$$

$$(\omega_0^2 + j\omega R - \omega^2)u_2 = \frac{1}{2}p(V_1 - jV_2) + Fs_2 \tag{9}$$

$$Q_1 = \frac{1}{2}p(u_1 + u_2) + C_0V_1 \tag{10}$$

$$Q_2 = \frac{-j}{2}p(u_1 - u_2) + C_0V_2 \tag{11}$$

where the generalized force for the traveling modes are expressed as

$$Fs_1 = \{\eta_1\}^*\{F\} \tag{12}$$
$$Fs_2 = \{\eta_2\}^*\{F\} \tag{13}$$

When $V_2 = -jV_1$, i.e. $V_1 = \cos(\omega t)$ and $V_2 = \sin(\omega t)$, only traveling wave mode 1 is excited.

2.2 The Rotor

The rotor is a narrow ring and pressed against the stator by a spring which provides a constant pressure. There is a thin layer of friction material between the rotor and the stator. The formulas of the rotor are similar to those of the stator but without the items related to the electric driving. The finite element approach provides the mode shapes and frequency of the rotor. The corresponding equations are written as

$$(\omega_{r0}^2 + j\omega R_r - \omega^2)u_{r1} = Fr_1 \tag{14}$$

and

$$Fr_1 = \{\eta_{r1}\}^*\{Fr\} \tag{15}$$

2.3 Interaction between the Stator and the Rotor

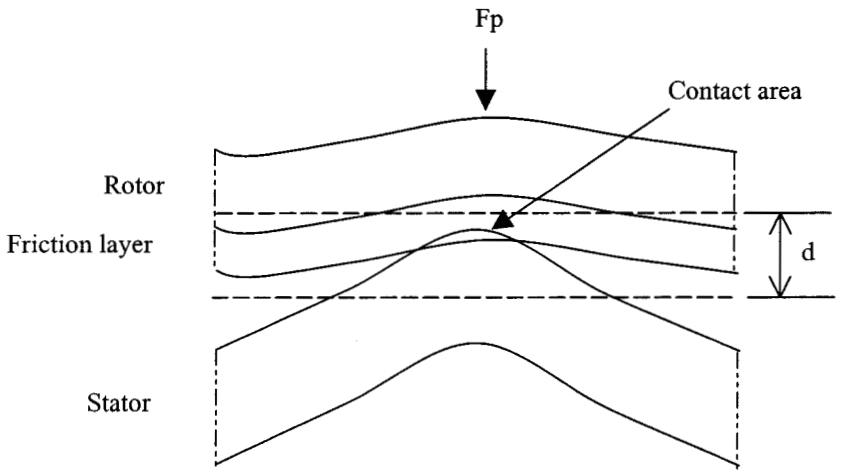

Figure 3: Interaction of the stator and the rotor via friction layer

The stator drives the rotor through a thin friction layer which is usually made by polymer. A constant force Fp presses the rotor against the stator. The penetration of the stator into the layer h_p is expressed as

$$h_p = w_s - w_r + h - d \tag{16}$$

where w_S and w_r are the normal displacements of the stator and the rotor respectively, h is the thickness of the friction layer, and d is the distance between the surfaces of the stator and the rotor. The normal displacement of the traveling wave in the rotor is present as

$$w_r = u_{r1} w_{r1} \tag{17}$$

where w_{r1} is the normal displacement of the traveling mode $\{\eta_{r1}\}$.

For simplicity, a brush model is used to calculate the normal pressure p developed in the contact area. The pressure is expressed as

$$p = \begin{cases} h_p E/h & h_p >= 0 \\ 0 & h_p < 0 \end{cases} \tag{18}$$

where E is the Yang's modulus of the material, and h is the thickness of the friction layer. The total normal force of the pressure is equal to the applied press force

$$\int p dA = F_p \tag{19}$$

There is also a friction force in tangent direction. Because that the tangent displacement of the mode on the rotor surface is small, the driviting effect of this force to the traveling wave on the rotor is neglected. Then, Eq.(14) becomes

$$(\omega_{r0}^2 + j\omega R_r - \omega^2) u_{r1} = \int w_{r1} p dA \tag{20}$$

For a given traveling wave in the stator w_S, the distance d, and then, the contact pressure p and wave amplitude u_{r1} can be determined by Eqs.(16) - (20).

The stator drivers the rotor to rotate by the friction force. The friction is described by Coulomb's law. Although the contact area may has slip and stick zones [Maeno T., 1994 and Wallashek J., 1998]. For simplicity, the sticking is neglected. We treat whole contact area as slip zone. The friction force exerted on the rotor in the contact area is

$$\tau = sign(v_s - v)\mu p \tag{21}$$

where μ is the friction coefficient, v_S is the velocity on the surface of the stator in tangent direction, and the v is rotor velocity due to rotation. The total driving force F_d is the integral of the friction force over the area,

$$F_d = \int \tau dA \tag{22}$$

The driving force or torque can be calculated by using this formula when the rotation speed in given.

The reaction of these interaction forces to the stator is represented by the item Fs_1 in Eq. (8). We have

$$Fs_1 = -(\int w_s^* p dA + \int v_s^* \tau dA) \tag{23}$$

Then, we can find the required driven voltage and current from Eq.(10) and (11).

3. RESULTS OF SAMPLE ULTRASONIC MOTOR

3.1 The 3D Model Analysis for the Stator

The commercial FE package ANSYS was used to analyze the stator. The modal analysis is used to determine the resonance frequencies and model shapes by assigning zero to [C], {F} and all V_e and solving the eigenvalue problem of Eq. (2) with constraint (3).

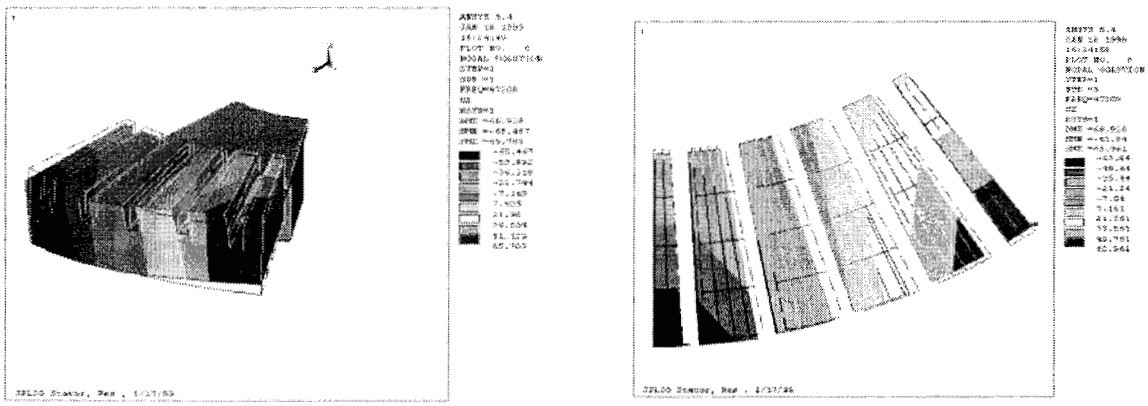

(a) 45° view (b) Top view of teeth

Figure 4: The modal shape for 1/2 wavelength sector

This 3D finite element model enables the simulation of complex structures and to obtain more accurate results than other approaches e.g. analytical models or annual finite element models. However, the computational process is time consuming and far from being practical when using a personal computers or workstations to determine the full model of the stator with finer meshes. Using the symmetry of the stator structure, a fraction of the stator mesh is needed combined with set proper boundary conditions allows significant reduction in computation time. In order to obtain high symmetry, 10 electrodes (polarized alternately) are assumed to be uniformly distributed on the circumference. Figure 4 shows the resonance frequency and the model shape obtained by meshing 1/10 of the stator, which is equal to 1/2

wavelength of the 5-wavelength mode. The volume is chosen with a total of 2340 mesh elements and total number of degree of freedom is 11000. Using a Sun workstation and an ANSYS program with these conditions the calculation time lasted 360 seconds. The computed resonance frequency of 47.208 kHz was found very close to the measured value of 47.29 kHz.

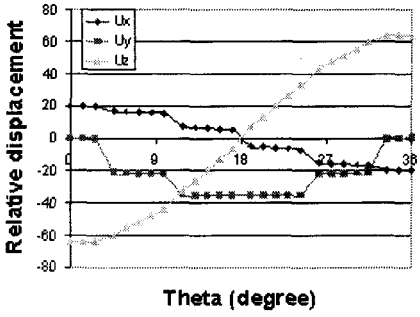

(a) At the outer diameter of the teeth

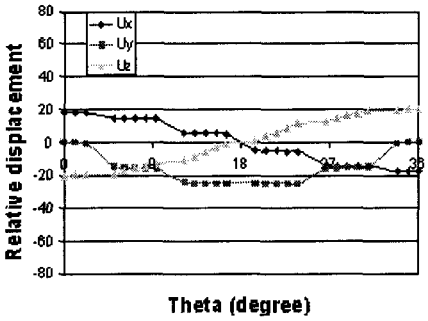

(b) At inner diameter of the teeth

Figure 5: Distribution of the displacements on the top surface of the teeth, Ux is in radial direction, Uy in circumference direction, and Uz is in axis direction.

The 3D model provides detailed displacement distribution of the mode on the tips of the teeth. The tip motion of the traveling wave is obtained by adding two vibration models separated by1/4 wavelength in space and 90° out of phase in time. As shown in the Figure 5, the radial displacements of the tips are comparable with the circumferential. The results also show that both normal and circumferential displacements at the inner diameter of the teeth are significantly less than those at the outer diameter. The ratio of the normal displacement over the circumferential is greatly changed as well. All these phenomena are important for motor design.

A comparison of the calculated input impedance to the measured is a common, convenient mean to evaluate the accuracy of the model. Although we can directly calculate the impedance curve by the FE package, but it requires full meshed model and long computing time. An alternative approach, the equivalent circuit, is used to get the curve.

The response of the stator at the frequency around the resonance can be presented by an equivalent circuit. The 3D finite element model was formulated for one terminal case, i.e. all the positively or negatively polarized areas are connected. In this case, the equivalent circuit is presented in Figures 6(a) and (b), where for this circuit there are two resonance frequencies. One is the series resonance F_s, which is equal to the resonance we computed by the 3D finite element model. The other is known as parallel resonance F_p. The F_p is computed in the same way as F_s in the 3D finite element model but without setting V_e to zero. At low frequency, the input impedance is a capacitance C^t given by

$$C^t = C_0 + C_{et}$$

where C_0 and C_{et} are the clumped and motion capacitance in the equivalent circuit of Figure 6(b) respectively.

Generally, the capacitance C^t can also be computed by the finite element model. The three parameters in Figure 6 (b) can be determined using the Electro-mechanical circuit. The stator actually has two electric input terminals; each is connected to partial electrodes. To obtain the equivalent circuit for the partial electrodes, the circuit in Figure 6(a) is redrawed as 6(c) to represent the case of two terminals. When the two terminals are connected in parallel, Figure 6(c) is

$$C_{el} = C_e\left(\frac{n}{m}\right)^2 \qquad L_{el} = L_e\left(\frac{m}{n}\right)^2$$

the same as 5(a). When the voltage is applied to one terminal and another is shorted, Figure 6(c) becomes 6(d). We have

$$C_1 = C_0 \frac{n}{m}$$

where m is the total number of the electrodes, and n is the number of effectived electrodes.

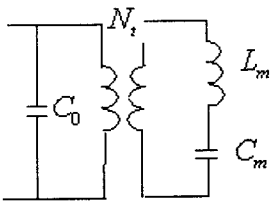

a. with one terminal

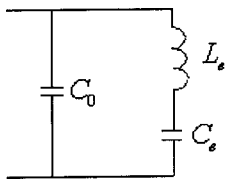

b. Electrical circuit

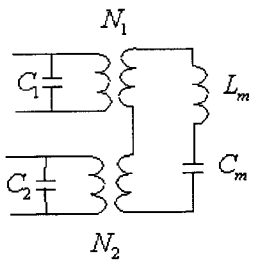

c. Electro-mechanical circuit with two terminals

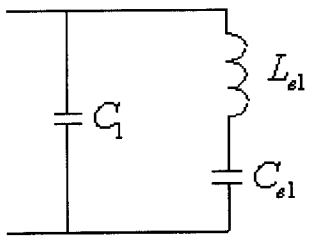

d. Electrical circuit with one of two terminals used

Figure 6: Equivalent circuit for the piezoelectric structure with one or two terminals

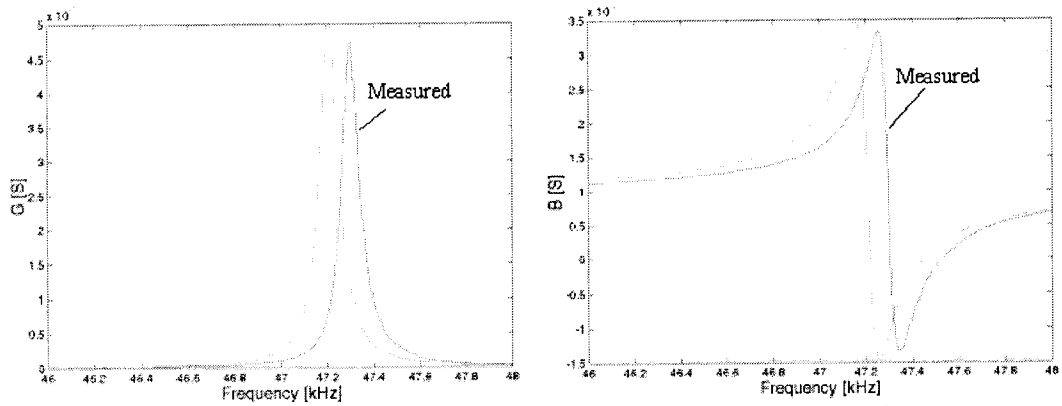

Figure 7: Computed electric impedance vesus measured

The input impedance is calculated according to the equivalent circuit after adding a resister to take in count the mechanical loss. The value of the resistance is determined by the measured Q_m. The result is shown in Figure 7 with the measured impedance. The main diference between the theoretical prediction and the experimental is a frequency shift of 0.1 kHz. This good agreement demonstrates the accurancy of the model.

3.2 The Rotor

The rotor is a narrow ring. A annular finite element model [Hagood et al] is used to get the mode shape and resonance frequency. The frequency is 58.06 kHz. The mode shape is shown in Figure 8.

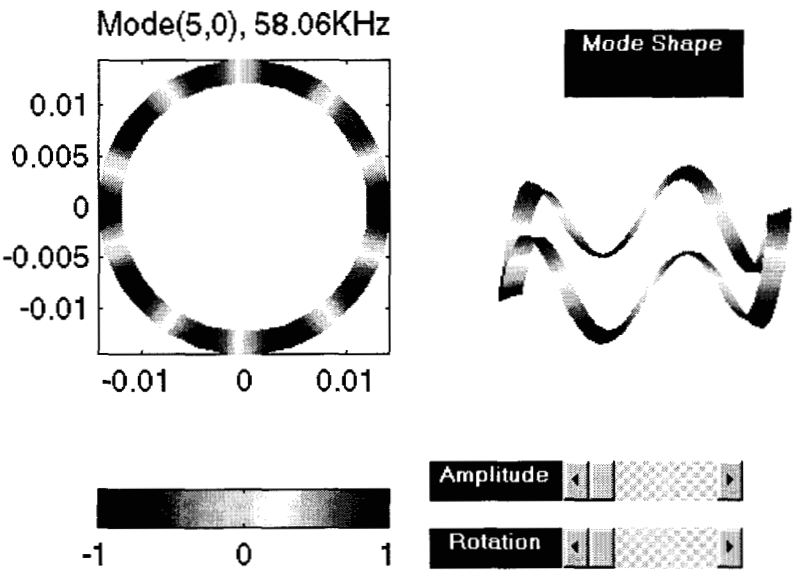

Figure 8: Mode shape and the frequency of the rotor

3.3 The Output Performance of the Motor

As shown in the Figure 2, there is an electrode to provide feedback signal to the driver. The signal is a measurement of wave amplitude on the stator. The electronic driver was designed to maintain the wave amplitude constant by adjusting frequency according to the feedback signal. The mechanical output performance, torque-speed and power-speed curves, under this driving condition are shown in Figure 9.

The computed result is presented in Figure 10. The normal force applied is 60 N. The measured value of friction coefficient is 0.16. The normal displacement of the wave is set as 2.5 μm. We do not have exact Yang's modulus of the friction material. It was chosen in reasonable range to get close result. In the computation, we further simplified the area integrals to line integrals by only taking the values at average radius of the contact area in account. The similarity of the computed and the measured implies that the simplified friction-driving model used in the modeling is close to the reality.

3. SUMMARY

A hybrid model that addressed a complete ultrasonic motor as a system was developed. The model uses a powerful commercial finite element package to express the dynamic characteristics of the stator and the rotor in engineering practice. An analog model was developed to couple the finite element model for the stator and rotor and it provides solution for the stator-interface layer-rotor system. Even though a simplified theoretical model was used for the interface layer, the model provides reasonably accurate results for CAD of the rotary ultrasonic motors. The computer model may be improved further by taking the stick-slit mechanism in the interface layer into account.

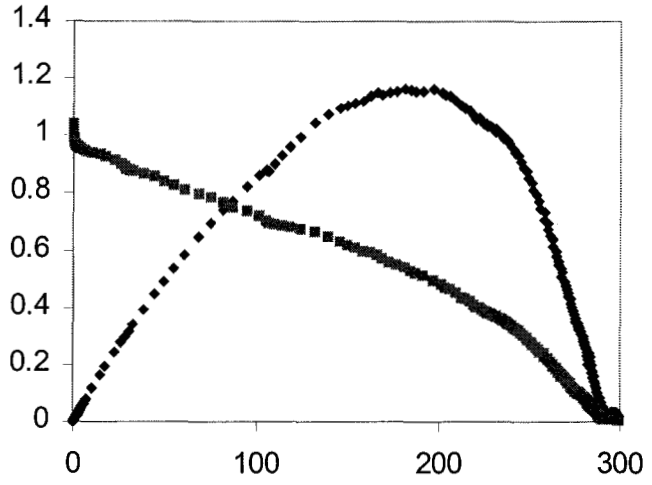

Figure 9: Measured motor performance

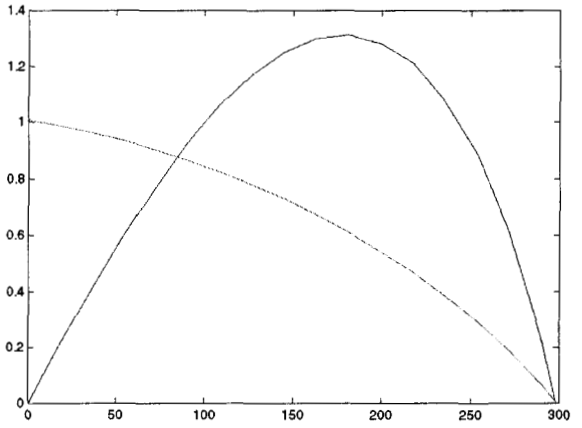

Figure 10: Computed motor performance

ACKNOWLEDGMENT

The results reported in this manuscript were obtained under the Planetary Dexterous Manipulator (PDM) Task, which is managed by Dr. Hari Das. PDM is a NASA Telerobotics task supported by a JPL, Caltech, contract with NASA Headquarters, Code S, Dave Lavery is the NASA HQ Program Manager and Dr. Chuck Weisbin is the JPL Program Manager.

REFERENCES

Allik H., and T.J.R. Hughes, "Finite Element Method for Piezoelectric Vibration," Int. J. Num. Math. Eng., Vol. 2, 1970, pp. 151-157.

Bao X., et al, "Vibration and acoustic radiation of piezoelectric transducers -- FEM-Equivalent circuit," Scietia Sinica Series A, Vol 26 1988, 1285-1294

Bar-Cohen Y., Bao X., and Grandia W., "Rotary Ultrasonic Motors Actuated By Traveling Flexural Waves," Proceedings of the SPIE International Smart Materials and Structures Conference, SPIE Paper No. 3668-63, New Port, CA, 1-5 March 1999.

Flynn A. M., et al, "Piezoelectric Micromotors for Microrobots" J. of MEMS, Vol. 1, No. 1, (1992), pp. 44-51.

Hagood N. and McFarland A, "Modeling of a piezoelectric rotary ultrasonic motor," IEEE UFFC, Vol. 42, (1992), pp. 210-214.

Hagedorn P, et al, "The importance of rotor flexibility in ultrasonic traveling wave motors," Smart Materials and Structures, Vol. 7, (1998), pp. 352-368.

Hollerbach M., I. W. Hunter and J. Ballantyne, "A Comparative Analysis of Actuator Technologies for Robotics." In Robotics Review 2, MIT Press, Edited by Khatib, Craig and Lozano-Perez (1991).

Inaba E., et al, "Piezoelectric Ultrasonic Motor," Proceedings of the IEEE Ultrasonics 1987 Symposium, pp. 747-756, (1987).

Kagawa K., T. Tsuchiya and T. Kataoka, "Finite Element Simulation of Dynamic Responses of Piezoelectric Actuators," J. of Sound and Vibrations, Vol. 89 (4), 1996, pp. 519-538.

Maeno T., et al, "Effect of the rotor/stator interface condition including contact type, geometry, and material on performance of ultrasonic motor," ASME, Vol. 116, (1994), pp. 726-732.

Wallashek J., "Piezoelectric Motors," J. of Intelligent Materials Systems and Structures, Vol. 6, (Jan. 1995), pp. 71-83.

Wallashek J., "Contact mechanics of piezoelectric ultrasonic motor," Smart Materials and Structures, Vol. 7, (1998), pp. 369-381.

Uchino K., "Piezoelectric ultrasonic motors: overview," Smart Materials and Structures, Vol. 7, (1998), pp. 273-285.